

Knowledge Transfer and Domain Adaptation for Fine-Grained Remote Sensing Image Segmentation

Shun Zhang^{1,*}, Xuechao Zou^{2,*}, Kai Li³, Congyan Lang², Shiyang Wang^{1,†}, Pin Tao^{1,3,†}, Tengfei Cao¹

¹School of Computer Technology and Applications, Qinghai University, Xining, China

²School of Computer Science and Technology, Beijing Jiaotong University, Beijing, China

³Department of Computer Science and Technology, Tsinghua University, Beijing, China

Abstract—Fine-grained remote sensing image segmentation is essential for accurately identifying detailed objects in remote sensing images. Recently, vision transformer models (VTM) pretrained on large-scale datasets have shown strong zero-shot generalization, indicating that they have learned the general knowledge of object understanding. We introduce a novel end-to-end learning paradigm combining knowledge guidance with domain refinement to enhance performance. We present two key components: the Feature Alignment Module (FAM) and the Feature Modulation Module (FMM). FAM aligns features from a CNN-based backbone with those from the pretrained VTM’s encoder using channel transformation and spatial interpolation, and transfers knowledge via KL divergence and L2 normalization constraint. FMM further adapts the knowledge to the specific domain to address domain shift. We also introduce a fine-grained grass segmentation dataset and demonstrate, through experiments on two datasets, that our method achieves a significant improvement of 2.57 mIoU on the grass dataset and 3.73 mIoU on the cloud dataset. The results highlight the potential of combining knowledge transfer and domain adaptation to overcome domain-related challenges and data limitations. The project page is available at <https://xavierjiezou.github.io/KTDA/>.

Index Terms—Fine-grained image segmentation, remote sensing, knowledge transfer, domain adaptation, vision transformer

I. INTRODUCTION

Remote sensing image segmentation is vital for applications such as environmental monitoring, agricultural surveys, and urban planning [1]–[3], particularly in the precise identification of fine-grained objects like grass, clouds, and crops at various levels. For example, in fine-grained cloud segmentation, it is not only necessary to detect whether an object is a cloud, but also to assess the thickness of its layers. As the volume and complexity of remote sensing data continue to increase, traditional segmentation methods [4]–[7] struggle to handle intricate and fine-grained objects. Consequently, enhancing the accuracy of remote sensing image segmentation, particularly for fine-grained tasks, has become an urgent challenge.

Recent advances in deep learning, especially convolutional neural networks (CNNs), have made significant strides in remote sensing image segmentation. More recently, vision transformers (VTMs) [8]–[10] have shown great potential in remote sensing image analysis due to their ability to model long-range dependencies. Large-scale pre-trained VTM models have demonstrated strong generalization across various vision tasks, offering valuable prior knowledge for remote sensing image segmentation. However, despite their success

on large-scale datasets [11], these models still face challenges in performing well on domain-specific remote sensing tasks, particularly in fine-grained object semantic segmentation.

There are significant domain differences between remote sensing images and general visual images. For example, remote sensing images have unique imaging characteristics, sensor types, resolutions, and scales, and the objects in these images often exhibit textures and structures that differ from those found in natural images. These differences make it difficult to directly apply pre-trained models designed for general visual tasks to remote sensing image segmentation, often leading to performance degradation when processing remote sensing data. Additionally, fine-grained objects in these images typically have small sizes and subtle details, further complicating the segmentation task.

To address these challenges, we propose an end-to-end learning framework that integrates knowledge transfer with domain adaptation. The framework features two key components: the Feature Alignment Module (FAM) and the Feature Modulation Module (FMM). FAM aligns features extracted by a CNN backbone with those from a pre-trained VTM encoder through channel transformation and spatial interpolation, enabling knowledge transfer via KL divergence, L2 normalization and auxiliary constraints. FMM then further adapts the transferred knowledge to the target domain to mitigate domain shift. Experimental results demonstrate that our method significantly improves segmentation performance, achieving a 2.57 mIoU gain on the grass dataset and a 3.73 mIoU gain on the cloud dataset, underscoring the effectiveness of combining knowledge transfer and domain adaptation to address challenges such as domain shift and data scarcity.

- We present a end-to-end learning paradigm that integrates knowledge transfer and domain adaptation for fine-grained remote sensing image segmentation. This framework effectively transfers knowledge from pre-trained models and adapts it to specific target domains.
- We propose two novel optimization strategies: knowledge transfer loss and domain adaptation loss. The former ensures a stable transition of feature distributions, while the latter mitigates domain shift.
- We develop two key components: the Feature Alignment Module (FAM), and the Feature Modulation Module (FMM). FAM aligns features extracted by a CNN backbone with those from a pre-trained VTM encoder. FMM

then further adapts features.

- We introduce the first fine-grained grass dataset that addresses challenges such as boundary ambiguity and misclassification. Our method achieves state-of-the-art results in fine-grained segmentation on two datasets.

II. RELATED WORK

A. Fine-Grained Remote Sensing Image Segmentation

Fine-grained segmentation refines semantic segmentation by distinguishing subcategories within classes, such as grass, shrubs, and trees under vegetation, which is critical for tasks like ecological monitoring. CNN-based models [4], [6], [7] leverage multi-scale for local modeling, while transformer-based models [9], [12], [13] enhance long-range dependency modeling. For tasks like cloud segmentation, methods such as [14], [15] address subtle distinctions. However, challenges persist due to limited fine-grained vegetation datasets, especially for grasslands, and the reliance on coarse classifications, highlighting the need for more advanced techniques.

B. Knowledge Distillation and Transfer Learning

Knowledge distillation, first introduced in [16], is a form of transfer learning where a smaller (student) model mimics a larger (teacher) model’s behavior using soft targets — probability distributions from the teacher. Recent works like MobileSAM [17] and EfficientSAM [18] apply this technique to transfer knowledge from SAM’s Image Encoder [19] to lightweight models, achieving high performance and fast inference for real-time applications. This aids in model compression and enhances generalization by transferring knowledge from a larger model. Transfer learning, a broader technique, involves adapting a pre-trained model to improve performance on related tasks, particularly with limited labeled data. This includes domain adaptation, where models are fine-tuned for specialized tasks, such as remote sensing image segmentation, by transferring knowledge from one domain to another.

C. Vision Transformers and Domain Adaptation

Vision Transformers (ViTs) [20], including SAM [19], DINOv2 [9], and MAE [21], demonstrate strong generalization across visual tasks due to their transformer-based architectures, which capture long-range dependencies and learn transferable features. However, when applied to specialized tasks, such as remote sensing image segmentation (e.g., grass, water, cloud detection), their performance may suffer due to the mismatch between general pre-training datasets and domain-specific features. Remote sensing images often contain unique visual attributes (e.g., lighting variations, complex spatial structures) not present in conventional datasets. Domain adaptation techniques address this by fine-tuning ViTs for specialized tasks, transferring knowledge from a source domain (e.g., general datasets) to a target domain (e.g., remote sensing images), thus improving segmentation performance.

III. METHOD

A. Knowledge Transfer

Knowledge transfer enables the CNN-based backbone to effectively learn from the encoder of the frozen vision transformer model (VTM), as shown in Fig. 1A. Specifically, Knowledge transfer is achieved through the combination of feature alignment and loss calculation. In the Feature Alignment Module (FAM), the multi-scale features from the backbone are aligned with those of the VTM by adjusting their channel dimensions and resizing the feature maps to match the VTM’s spatial resolution.

1) *Feature Alignment Module*: The FAM is a simple yet highly effective component. Given an input image $x \in \mathbb{R}^{C \times H \times W}$, where C represents the number of channels, H is the height, and W is the width, the backbone generates multi-scale features: $\{F_1, F_2, \dots, F_n\}$, $F_i \in \mathbb{R}^{C_i \times H_i \times W_i}$, n denotes the number of features. FAM begins by adjusting the channel depth of each feature map using 1×1 convolutions, denoted as \mathcal{C} , to produce aligned feature maps:

$$F'_i = \mathcal{C}_i(F_i). \quad (1)$$

Next, bilinear interpolation is applied to resize the feature maps, aligning their spatial resolution with that of the VTM’s feature maps:

$$F''_i = \mathcal{O}(F'_i, H_{\text{VTM}}, W_{\text{VTM}}),$$

where \mathcal{O} denotes bilinear interpolation. This straightforward alignment process facilitates effective transfer learning by enabling the transfer of knowledge from the VTM to the backbone, improving domain adaptation with minimal computational overhead.

2) *Loss Function*: The loss function for transfer learning is designed to minimize the discrepancy between the feature representations of the backbone and the Vision Transformer Model (VTM) after feature alignment. Following the multi-scale feature alignment through the Feature Alignment Module (FAM), the feature maps from both the backbone and the VTM are paired. The transfer learning loss is computed by combining the \mathcal{L}_{mse} and \mathcal{L}_{kl} losses to enhance model optimization and regularization.

The loss at each scale is calculated using both \mathcal{L}_{mse} and \mathcal{L}_{kl} as follows:

$$\mathcal{L}_{\text{mse}} = \frac{1}{N} \sum_{i=1}^N \|F''_i - F_{\text{VTM}}\|_2^2, \mathcal{L}_{\text{kl}} = \frac{1}{N} \sum_{i=1}^N \text{KL}(F''_i \| F_{\text{VTM}}), \quad (2)$$

where F''_i denotes the feature map at the i -th scale, and F_{VTM} represents the feature map from the VTM. The terms \mathcal{L}_{mse} and \mathcal{L}_{kl} are computed by averaging over all scales to ensure consistent alignment between the backbone and VTM across different resolutions.

The combined loss, \mathcal{L}_{kt} , is a weighted sum of \mathcal{L}_{mse} and \mathcal{L}_{kl} :

$$\mathcal{L}_{\text{kt}} = \lambda_{\text{mse}} \cdot \mathcal{L}_{\text{mse}} + \lambda_{\text{kl}} \cdot \mathcal{L}_{\text{kl}}, \quad (3)$$

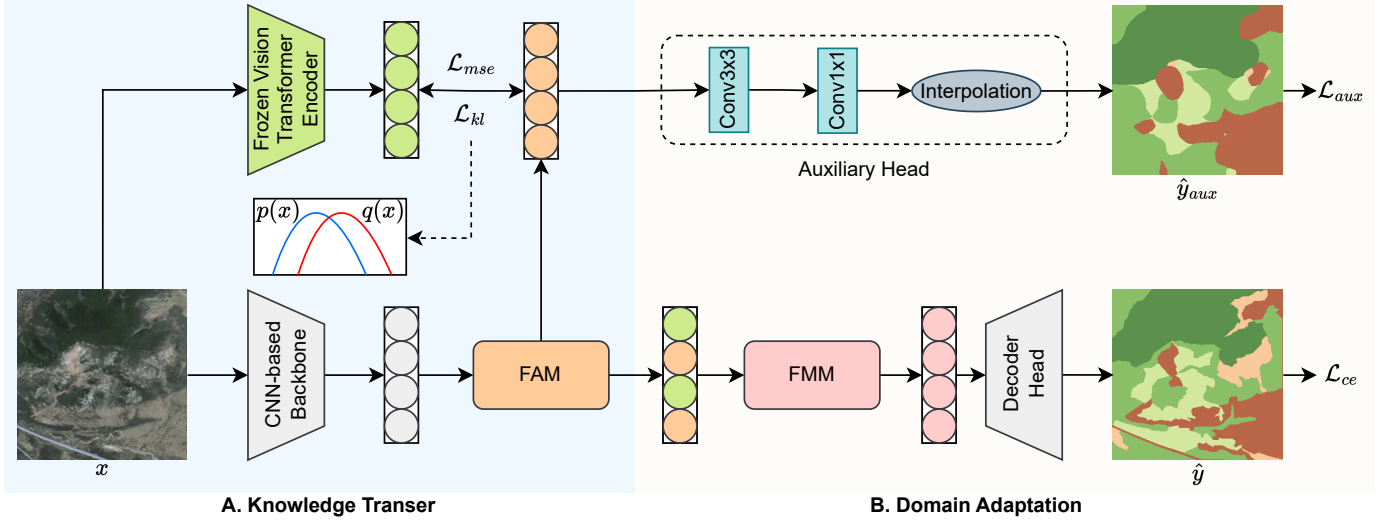


Fig. 1. Overview of the proposed framework that integrates knowledge transfer and domain adaptation for fine-grained remote sensing image segmentation.

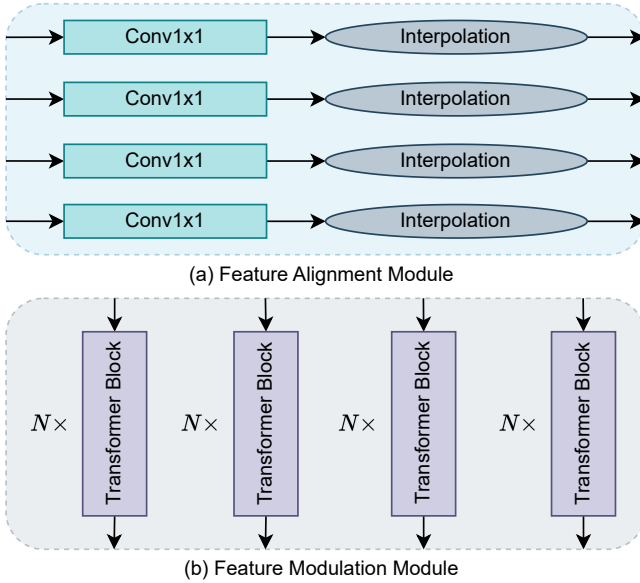


Fig. 2. Detailed structure of the FAM and FMM.

where $\lambda_{mse} = 0.5$ and $\lambda_{kl} = 0.5$. This loss function combines the \mathcal{L}_{kl} and \mathcal{L}_{mse} to enhance feature alignment and knowledge transfer between the backbone and the VTM.

B. Domain Adaptation

Domain Adaptation involves a Feature Modulation Module (FMM) built upon Transformer blocks to align the feature distribution between the source and target domains. The module processes the input features $F'' \in \mathbb{R}^{C \times H \times W}$ through N sequential Transformer blocks, progressively adapting the feature distribution to better match the target domain. A dual-decoder architecture is employed, with the primary UperNet decoder optimized through a weighted combination of cross-

entropy losses, thereby enhancing the model's performance in domain adaptation tasks.

1) *Feature Modulation Module*: The FMM is also a simple yet effective approach for adapting the feature distribution from a general dataset to a target dataset using Transformer blocks. Given the feature map $F'' \in \mathbb{R}^{C \times H \times W}$ from the FAM, the module applies N Transformer blocks to modulate the features.

The output of the k -th Transformer Block (TB) is computed as:

$$F^{(k)} = \text{TB}_k(F^{(k-1)}), \quad k \in \{1, \dots, N\}, \quad F^{(0)} = F'',$$

where each Transformer Block consists of a self-attention mechanism and a feedforward neural network. The final output, $F^{(N)} \in \mathbb{R}^{C \times H \times W}$, represents the transformed feature map, aligned with the target domain's distribution. This simple yet powerful mechanism effectively facilitates domain adaptation, ensuring that the features from the general dataset are well-aligned with the target dataset for improved performance.

2) *Loss Function*: The loss function for domain adaptation in semantic segmentation is designed based on the outputs from the FMM. After passing through N Transformer blocks, the feature map $F^{(N)}$ is processed by the decoder head (\hat{y}) to produce the predicted segmentation output.

The domain adaptation loss, \mathcal{L}_{da} , consists of two parts: the cross-entropy loss \mathcal{L}_{ce} calculated from the decoder head's output, and the auxiliary loss \mathcal{L}_{aux} calculated from the auxiliary head. These components are defined as follows:

$$\mathcal{L}_{ce} = \text{CE}(\hat{y}, y), \quad \mathcal{L}_{aux} = \text{CE}(\hat{y}_{aux}, y), \quad (4)$$

where \hat{y} represents the predicted segmentation output, y is the ground truth label, and \hat{y}_{aux} is the predicted output from the auxiliary head.

The domain adaptation loss \mathcal{L}_{da} is the weighted sum of these two components:

$$\mathcal{L}_{da} = \lambda_{ce} \cdot \mathcal{L}_{ce} + \lambda_{aux} \cdot \mathcal{L}_{aux}, \quad (5)$$

where $\lambda_{ce} = 1.0$ and $\lambda_{aux} = 0.4$.

The total loss for the domain adaptation task combines both the knowledge transfer loss \mathcal{L}_{kt} and the domain adaptation loss \mathcal{L}_{da} as follows:

$$\mathcal{L}_{total} = \lambda_{kt} \cdot \mathcal{L}_{kt} + \lambda_{da} \cdot \mathcal{L}_{da}, \quad (6)$$

where $\lambda_{kt} = \lambda_{da} = 1.0$ and \mathcal{L}_{kt} is the loss defined in the previous section and \mathcal{L}_{da} includes both the cross-entropy loss and the auxiliary loss for domain adaptation. The total loss function allows the model to simultaneously optimize knowledge transfer and domain adaptation, improving performance on the target dataset.

IV. EXPERIMENT

A. Datasets

1) *Fine-Grained Grass Segmentation*: We have developed a fine-grained grass dataset to improve the accuracy of grass-land extraction in complex terrains. Existing datasets [22]–[25] lack detailed labeling, limiting their ability to address challenges like boundary ambiguity and misclassification. Our dataset fills this gap by offering a more refined classification, which enhances grass segmentation and contributes to a better understanding of grass ecosystems.

The dataset was created using high-resolution (8m) satellite imagery from the Gaofen series (Gaofen-2 and Gaofen-6), captured in 2019 over Maduo County, China, located in the Yellow River source area. This region is known for its high-altitude, alpine grasslands, and complex terrain, with coordinates between 33°50′–35°40′ N latitude and 96°50′–99°20′ E longitude. We collected two 13,872 × 13,150-pixel images from Gaofen-6 and two 7,300 × 6,905-pixel images from Gaofen-2, all containing red, green, and blue spectral bands. These images provide critical information for fine-grained grass extraction. Labeling was assisted by the X-AnyLabeling¹ tool, supplemented with manual refinements to ensure high accuracy. Grassland coverage was classified into five levels, based on national grassland survey standards: low coverage (<10%), medium-low coverage (10%-25%), medium coverage (25%-50%), medium-high coverage (50%-75%), and high coverage (>75%), as shown in Tab. I. The final dataset comprises 1,500 pairs of 256 × 256 patches, split into training and testing sets with an 8:2 ratio. This dataset, with its detailed and accurate labeling, is a valuable resource for advancing remote sensing applications, particularly in ecologically sensitive and high-altitude regions like the Yellow River source area.

2) *Fine-Grained Cloud Segmentation*: The dataset [26] consists of 96 terrain-corrected (Level-1T) scenes from Landsat 8 OLI and TIRS, covering diverse biomes. This variety supports cloud detection and removal in complex environments. The dataset includes manually generated cloud masks with pixel-level annotations for cloud shadow, clear sky, thin clouds,

TABLE I
COVERAGE LEVELS AND PIXEL COUNT

Level	Coverage	Range (%)	Pixels
I	Low	< 10	12,680,802
II	Middle-Low	10-25	13,598,315
III	Middle	25-50	9,744,128
IV	Middle-High	50-75	7,919,316
V	High	> 75	31,489,375

and cloud areas. Each scene is cropped into 512×512 pixel patches and split into training, validation, and test sets (6:2:2 ratio). It is a valuable resource for training and evaluating cloud detection models across various terrains.

B. Implementation Details

1) *Hyperparameter and Training Settings*: All experiments were conducted using the MMsegmentation², running on 8 NVIDIA A100 GPUs. Our experiment employed UPerNet [27] as the default decoder head and FCN [4] as the auxiliary head, unless specified otherwise. The experiments were trained for a maximum of 23,000 iterations. The optimizer used for training was AdamW [28] with an initial learning rate of 1×10^{-3} , with a custom learning rate schedule. The learning rate started with a linear warm-up over the first 1,150 iterations, followed by a PolyLR scheduler with a minimum eta value of 0.0 and a power parameter set to 0.9. The learning rate decay continued until the end of the iteration. The batch size was set to 4.

2) *Baselines and Evaluation Metrics*: To comprehensively evaluate the performance of our proposed method, we compare it with several widely recognized segmentation models. For the grass datasets, we use the following models as baselines: FCN [4], PSPNet [6], DeepLabV3+ [7], SegFormer [12], Mask2Former [13], DINOv2 [9], and U-Net [5]. For the cloud dataset, we use models specifically designed for cloud segmentation: SCNN [29], CDNetV1 [14], CDNetV2 [15], MCDNet [30], UNetMobV2 [31], HRcloudNet [32], and KappaMask [33]. All of feature extraction networks are pre-trained on the ImageNet [11], ensuring a fair comparison. We evaluate segmentation performance using three standard metrics: Mean Intersection over Union (mIoU), F1 Score, and Overall Accuracy (OA), all reported as percentages (%).

C. Ablation and Discussion

1) *Study of Loss on Knowledge Transfer*: Tab. II shows the impact of every loss functions on knowledge transfer from the Frozen Vision Transformer Encoder [9]. The best performance is achieved by combining all loss items, reaching a mIoU of 50.81%, OA of 74.10%, and F1 score of 64.91%. Among these components, \mathcal{L}_{kl} demonstrates the most significant impact, as evidenced by the substantial performance drop when it is removed (mIoU decreases by 7.13%). Removing the \mathcal{L}_{aux} results in a relatively minor performance decline (mIoU drops by 1.21%), while excluding \mathcal{L}_{mse} leads to a moderate decrease

¹<https://github.com/CVHub520/X-AnyLabeling>

²<https://github.com/open-mmlab/msegmentation>

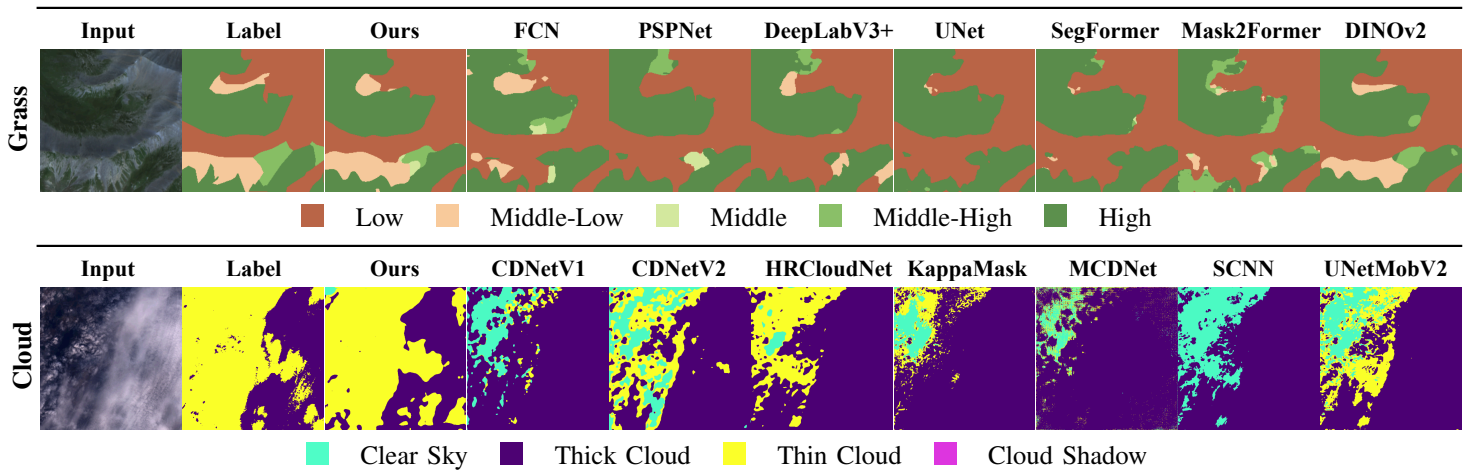


Fig. 3. Comparison of visualization segmentation results of different models on the fine-grained grass and cloud segmentation datasets.

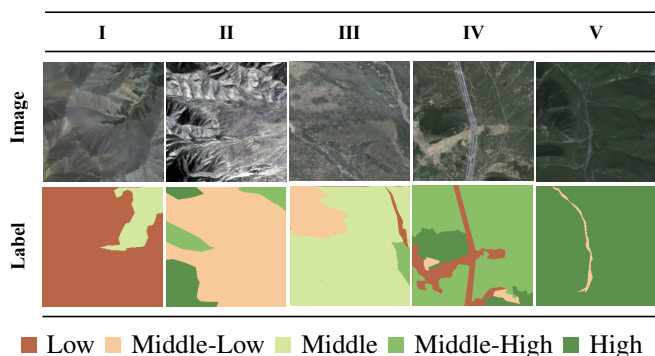


Fig. 4. Each level of labeling, based on category Naming Based on 70% Pixel Proportion.

TABLE II
COMPARISON OF DIFFERENT LOSS COMPONENTS AND THE PRESENCE OF AN AUXILIARY HEAD IN THE PROPOSED SEMANTIC SEGMENTATION MODEL.

Knowledge Transfer		Domain Adaptation		Metrics		
\mathcal{L}_{kl}	\mathcal{L}_{mse}	\mathcal{L}_{aux}	\mathcal{L}_{ce}	mIoU \uparrow	OA \uparrow	F1 \uparrow
✓	✓	✓	✓	50.81	74.10	64.91
✓	✓	×	✓	49.60	73.30	63.75
✓	×	✓	✓	49.18	72.78	63.34
×	✓	✓	✓	43.68	68.71	57.41

(mIoU reduces by 1.63%). These results indicate that \mathcal{L}_{kl} plays a crucial role in effective knowledge transfer from the knowledge of the pre-trained vision transformer encoder.

2) *Impact of FAM on Knowledge Transfer*: Tab. III illustrates the effect of the Feature Alignment Module and the knowledge transfer loss, which combines \mathcal{L}_{kl} , \mathcal{L}_{mse} , and \mathcal{L}_{aux} , on knowledge transfer. Incorporating FAM with multi-scale outputs consistently improves performance, with mIoU increasing from 47.88% to 49.00%. When FAM is combined with the \mathcal{L}_{aux} , the best performance is achieved, with mIoU reaching 49.29%, OA of 73.19%, and F1 score of 63.38%.

TABLE III
EFFECT OF FEATURE ALIGNMENT MODULE (FAM) AND $\mathcal{L}_{kl} + \mathcal{L}_{mse}$ ON KNOWLEDGE TRANSFER.

FAM	mIoU \uparrow	OA \uparrow	F1 \uparrow
Single-Scale	47.88	71.43	62.25
Multi-Scale	49.00	73.27	62.89
×	47.57	71.54	61.7
✓ (w/o loss)	48.64	73.10	62.51
✓ (w/ loss)	49.29	73.19	63.38

TABLE IV
STUDY ON THE NUMBER OF TRANSFORMER BLOCKS IN THE FMM.

N	mIoU \uparrow	OA \uparrow	F1 \uparrow
0	48.82	72.76	62.95
1	49.90	73.21	64.08
2	50.57	73.62	64.78
3	49.64	73.27	63.78
4	50.86	74.26	65.01

These results highlight that the improvement is not solely due to an increase in the number of parameters introduced by FAM, but rather the synergistic effect of the knowledge transfer loss, which plays a crucial role in enhancing knowledge transfer and improving segmentation accuracy.

3) *Impact of FMM on Domain Adaptation*: Tab. IV shows the effect of the Feature Modulation Module on domain adaptation. As the number of Transformer Blocks in FMM increases, with the best results achieved at $N=4$, reaching mIoU of 50.86%, OA of 74.26%, and F1 score of 65.01%. The performance slightly declines beyond $N=2$, indicating diminishing returns. These results highlight the effectiveness of FMM in enhancing domain adaptation, with $N=4$ providing the optimal performance.

D. Comparison with State-of-the-Art Methods

1) *Quantitative Analysis*: We perform a comprehensive evaluation of our method by comparing it with state-of-

TABLE V
THE PERFORMANCE COMPARISON OF DIFFERENT METHODS ON OUR FINE-GRAINED GRASS SEGMENTATION DATASET.

Method	mIoU \uparrow	OA \uparrow	F1 \uparrow
FCN [4]	47.47	67.85	61.99
PSPNet [6]	47.95	69.12	62.55
DeepLabV3+ [7]	47.95	68.97	62.50
UNet [5]	48.17	69.77	62.34
SegFormer [12]	48.29	68.93	62.82
Mask2Former [13]	44.93	65.90	58.91
DINOv2 [9]	47.57	71.54	61.70
Ours	50.86	74.26	65.01

TABLE VI
THE PERFORMANCE COMPARISON OF DIFFERENT METHODS ON THE FINE-GRAINED CLOUD SEGMENTATION DATASET.

Method	mIoU \uparrow	OA \uparrow	F1 \uparrow
MCDNet [30]	33.85	69.75	42.76
SCNN [29]	32.38	71.22	52.41
CDNetv1 [14]	34.58	68.16	45.80
KappaMask [33]	42.12	76.63	68.47
UNetMobv2 [31]	47.76	82.00	56.91
CDNetv2 [15]	43.63	78.56	70.33
HRCLOUDNet [32]	43.51	77.04	71.36
Ours	51.49	83.55	60.08

the-art approaches on two fine-grained segmentation tasks: grass segmentation and cloud segmentation. The evaluation metrics include mean Intersection over Union (mIoU), overall accuracy (OA), and F1-score. The detailed performance comparisons are shown in Tab. V and Tab. VI.

For grass segmentation, our method significantly outperforms existing techniques across all metrics, as presented in Tab. V. Specifically, we achieve a mIoU of 50.86, OA of 74.26, and F1-score of 65.01, surpassing the next best method, DINOv2 [9], which reports a mIoU of 47.57, OA of 71.54, and F1-score of 61.70. Other methods, such as FCN [4], PSPNet [6], and DeepLabV3+ [7], show lower performance, with mIoU values ranging from 44.93 to 47.95.

Similarly, in the cloud segmentation task, our approach achieves superior results, as shown in Tab. VI. We attain a mIoU of 51.49, OA of 83.55, and F1-score of 60.08, outperforming the previous best method, HRCLOUDNet [32], which achieves a mIoU of 43.51, OA of 77.04, and F1-score of 71.36. While methods like UNetMobv2 [31] and KappaMask [33] also show competitive results, they fall short in comparison to our method, with mIoU values of 47.76 and 42.12, respectively.

Our approach thus demonstrates strong performance and significant improvements over existing methods on both the grass and cloud segmentation tasks, highlighting its effectiveness in handling fine-grained segmentation challenges.

2) *Visualization Results*: We present a qualitative comparison of our method with state-of-the-art approaches on two fine-grained segmentation tasks: grass segmentation and cloud segmentation. The visualization results are shown in Fig. 3, where we provide segmented outputs for various models,

highlighting the differences in performance.

For the grass segmentation task, shown in the top part of Fig. 3, our model produces more accurate and detailed segmentations across different grass density levels, ranging from low to high. The segmentation boundaries are sharper, and finer details are captured compared to the other methods, which tend to blur the transitions between different regions. This is especially noticeable in areas with dense or sparse grass, where our method effectively distinguishes subtle variations in the vegetation.

In the cloud segmentation task, presented in the bottom part of Fig. 3, our method excels in distinguishing various cloud types, such as clear sky, thick cloud, thin cloud, and cloud shadow. The segmentation results are more precise, with better handling of complex cloud patterns and clearer differentiation between the cloud and sky regions. Compared to other models, which struggle with complex cloud formations and shadowed areas, our approach shows a more accurate delineation, particularly for thin clouds and cloud shadows.

Overall, the visualization results demonstrate the superiority of our method in producing fine-grained and accurate segmentations for both grass and cloud segmentation tasks, highlighting its effectiveness in handling complex and varied data.

V. CONCLUSION

This paper presents an innovative approach for fine-grained remote sensing image segmentation by combining knowledge transfer and domain adaptation. Through the integration of the feature alignment module and feature modulation module, our method effectively leverages pretrained vision transformers to enhance segmentation accuracy. Experiments on two datasets, including the novel fine-grained grass segmentation dataset, demonstrate significant improvements in performance, showcasing the effectiveness of knowledge transfer and domain adaptation in addressing domain shift and data limitations.

REFERENCES

- [1] Runmin Dong, Lichao Mou, Mengxuan Chen, Weijia Li, Xin-Yi Tong, Shuai Yuan, Lixian Zhang, Juepeng Zheng, Xiaoxiang Zhu, and Hao-huan Fu, "Large-scale land cover mapping with fine-grained classes via class-aware semi-supervised semantic segmentation," in *ICCV*, 2023, pp. 16783–16793.
- [2] Yaqi Han, Xinyi Yang, Tian Pu, and Zhenming Peng, "Fine-grained recognition for oriented ship against complex scenes in optical remote sensing images," *TGRS*, vol. 60, pp. 1–18, 2021.
- [3] Rui Li, Shunyi Zheng, Ce Zhang, Chenxi Duan, Jianlin Su, Libo Wang, and Peter M Atkinson, "Multiattention network for semantic segmentation of fine-resolution remote sensing images," *TGRS*, vol. 60, pp. 1–13, 2021.
- [4] Jonathan Long, Evan Shelhamer, and Trevor Darrell, "Fully convolutional networks for semantic segmentation," in *CVPR*, 2015, pp. 3431–3440.
- [5] Olaf Ronneberger, Philipp Fischer, and Thomas Brox, "U-net: Convolutional networks for biomedical image segmentation," in *MICCAI*. Springer, 2015, pp. 234–241.
- [6] Hengshuang Zhao, Jianping Shi, Xiaojuan Qi, Xiaogang Wang, and Jiaya Jia, "Pyramid scene parsing network," in *CVPR*, 2017, pp. 2881–2890.
- [7] Liang-Chieh Chen, Yukun Zhu, George Papandreou, Florian Schroff, and Hartwig Adam, "Encoder-decoder with atrous separable convolution for semantic image segmentation," in *ECCV*, 2018, pp. 801–818.

- [8] Haoxiang Wang, Pavan Kumar Anasosalu Vasu, Fartash Faghri, Raviteja Vemulapalli, Mehrdad Farajtabar, Sachin Mehta, Mohammad Rastegari, Oncel Tuzel, and Hadi Pouransari, "Sam-clip: Merging vision foundation models towards semantic and spatial understanding," in *CVPR*, 2024, pp. 3635–3647.
- [9] Maxime Oquab, Timothée Darcet, and Théo et al. Moutakanni, "DI-NOv2: Learning Robust Visual Features without Supervision," *TMLR*, pp. 1–31, 2024.
- [10] Alec Radford, Jong Wook Kim, and Chris et al. Hallacy, "Learning transferable visual models from natural language supervision," in *ICML*, 2021, vol. 139, pp. 8748–8763.
- [11] Olga Russakovsky, Jia Deng, Hao Su, Jonathan Krause, Sanjeev Satheesh, Sean Ma, Zhiheng Huang, Andrej Karpathy, Aditya Khosla, Michael Bernstein, et al., "Imagenet large scale visual recognition challenge," *IJCV*, vol. 115, pp. 211–252, 2015.
- [12] Enze Xie, Wenhui Wang, Zhiding Yu, Anima Anandkumar, Jose M. Alvarez, and Ping Luo, "Segformer: Simple and efficient design for semantic segmentation with transformers," in *NeurIPS*, 2021, vol. 34, pp. 12077–12090.
- [13] Bowen Cheng, Ishan Misra, Alexander G Schwing, Alexander Kirillov, and Rohit Girdhar, "Masked-attention mask transformer for universal image segmentation," in *CVPR*, 2022, pp. 1290–1299.
- [14] Jingyu Yang, Jianhua Guo, Huanjing Yue, Zhiheng Liu, Haofeng Hu, and Kun Li, "Cdnnet: Cnn-based cloud detection for remote sensing imagery," *TGRS*, vol. 57, no. 8, pp. 6195–6211, 2019.
- [15] Jianhua Guo, Jingyu Yang, Huanjing Yue, Hai Tan, Chunping Hou, and Kun Li, "Cdnnetv2: Cnn-based cloud detection for remote sensing imagery with cloud-snow coexistence," *TGRS*, vol. 59, no. 1, pp. 700–713, 2021.
- [16] Geoffrey Hinton, Oriol Vinyals, and Jeff Dean, "Distilling the knowledge in a neural network," in *NeurIPS*, 2014, pp. 1–9.
- [17] Chaoning Zhang, Dongshen Han, Yu Qiao, Jung Uk Kim, Sung-Ho Bae, Seungkyu Lee, and Choong Seon Hong, "Faster segment anything: Towards lightweight sam for mobile applications," *arXiv preprint arXiv:2306.14289*, 2023.
- [18] Yunyang Xiong, Bala Varadarajan, Lemeng Wu, Xiaoyu Xiang, Fanyu Xiao, Chenchen Zhu, Xiaoliang Dai, Dilin Wang, Fei Sun, Forrest Iandola, et al., "Efficientsam: Leveraged masked image pretraining for efficient segment anything," in *CVPR*, 2024, pp. 16111–16121.
- [19] Alexander Kirillov, Eric Mintun, and Nikhila et al. Ravi, "Segment anything," in *ICCV*, 2023, pp. 4015–4026.
- [20] Alexey Dosovitskiy, Lucas Beyer, Alexander Kolesnikov, Dirk Weissenborn, Xiaohua Zhai, Thomas Unterthiner, Mostafa Dehghani, Matthias Minderer, Georg Heigold, Sylvain Gelly, et al., "An image is worth 16x16 words: Transformers for image recognition at scale," in *ICLR*, 2020, pp. 1–21.
- [21] Kaiming He, Xinlei Chen, Saining Xie, Yanghao Li, Piotr Dollár, and Ross Girshick, "Masked autoencoders are scalable vision learners," in *CVPR*, 2022, pp. 16000–16009.
- [22] Patrick Helber, Benjamin Bischke, Andreas Dengel, and Damian Borth, "Eurosat: A novel dataset and deep learning benchmark for land use and land cover classification," *IEEE J-STARs*, 2019.
- [23] Xin-Yi Tong, Gui-Song Xia, Qikai Lu, Huanfeng Shen, Shengyang Li, Shucheng You, and Liangpei Zhang, "Land-cover classification with high-resolution remote sensing images using transferable deep models," *RSE*, vol. 237, pp. 111322, 2020.
- [24] Adrian Boguszewski, Dominik Batorski, Natalia Ziemia-Jankowska, Tomasz Dziedzic, and Anna Zambrzycka, "Landcover.ai: Dataset for automatic mapping of buildings, woodlands, water and roads from aerial imagery," in *CVPR*, June 2021, pp. 1102–1110.
- [25] Ronald Kemker, Carl Salvaggio, and Christopher Kanan, "Algorithms for semantic segmentation of multispectral remote sensing imagery using deep learning," *ISPRS J. Photogramm. Remote Sens.*, 2018.
- [26] Steve Foga, Pat L Scaramuzza, Song Guo, Zhe Zhu, Ronald D Dille Jr, Tim Beckmann, Gail L Schmidt, John L Dwyer, M Joseph Hughes, and Brady Laue, "Cloud detection algorithm comparison and validation for operational landsat data products," *RSE*, vol. 194, pp. 379–390, 2017.
- [27] Tete Xiao, Yingcheng Liu, Bolei Zhou, Yuning Jiang, and Jian Sun, "Unified perceptual parsing for scene understanding," in *ECCV*, 2018, pp. 418–434.
- [28] Ilya Loshchilov and Frank Hutter, "Decoupled weight decay regularization," in *ICLR*, 2018.
- [29] Dengfeng Chai, Jingfeng Huang, Minghui Wu, Xiaoping Yang, and Ruisheng Wang, "Remote sensing image cloud detection using a shallow convolutional neural network," *ISPRS J. Photogramm. Remote Sens.*, vol. 209, pp. 66–84, 2024.
- [30] Junwu Dong, Yanhui Wang, Yang Yang, Mengqin Yang, and Jun Chen, "Mcdnet: Multilevel cloud detection network for remote sensing images based on dual-perspective change-guided and multi-scale feature fusion," *JAG*, vol. 129, pp. 103820, 2024.
- [31] Cesar Aybar, Luis Ysuhuaylas, Jhomira Loja, Karen Gonzales, Fernando Herrera, Lesly Bautista, Roy Yali, Angie Flores, Lissette Diaz, Nicole Cuenca, et al., "Cloudsen12, a global dataset for semantic understanding of cloud and cloud shadow in sentinel-2," *Scientific data*, vol. 9, no. 1, pp. 782, 2022.
- [32] Jingsheng Li, Tianxiang Xue, Jiayi Zhao, Jingmin Ge, Yufang Min, Wei Su, and Kun Zhan, "High-resolution cloud detection network," *JEL*, vol. 33, no. 4, pp. 043027–043027, 2024.
- [33] Marharya Domnich, Indrek Sünter, Heido Trofimov, Olga Wold, Fariha Harun, Anton Kostiuukhin, Mihkel Järveoja, Mihkel Veske, Tanel Tamm, Kaupo Voormansik, et al., "Kappamask: Ai-based cloudmask processor for sentinel-2," *Remote Sensing*, vol. 13, no. 20, pp. 4100, 2021.